applied sciences

MDPI

Review

Brief Review of Recent Developments in Fiber Lasers

Galina Nemova

Department of Engineering Physics, Polytechnique Montréal, P.O. Box 6079, Station Centre-Ville, Montreal, QC H3C 3A7, Canada; galina.nemova@videotron.ca

Abstract: This review covers the recent achievements in high-power rare earth (RE)-doped fiber lasers, Raman fiber lasers, and Brillouin fiber lasers. RE-doped fiber lasers have many applications such as laser cutting, laser welding, laser cleaning, and laser precision processing. They operate in several wavelength ranges including 1050–1120 nm (ytterbium-doped fiber lasers), 1530–1590 nm (erbium- and erbium–ytterbium-doped fiber lasers), and 1900–2100 nm (thulium- and holmium-doped fiber lasers). White spaces in the wavelength spectrum, where no RE-doped fiber lasers are available, can be covered by Raman lasers. The heat power generated inside the laser active medium due to the quantum defect degrades the performance of the laser causing, for example, transverse-mode instability and thermal lensing. It can even cause catastrophic fiber damage. Different approaches permitting the mitigation of the heat generation process are considered in this review. Brillouin fiber lasers, especially multiwavelength Brillouin fiber lasers, have several important applications including optical communication, microwave generation, and temperature sensing. Recent progress in Brillouin fiber lasers is considered in this review.

Keywords: fiber laser; rare earth-doped fiber laser; Raman laser; Brillouin fiber laser; radiation-balanced fiber laser

Citation: Nemova, G. Brief Review of Recent Developments in Fiber Lasers. *Appl. Sci.* **2024**, *14*, 2323. https://doi.org/10.3390/app14062323

Academic Editor: Giampiero Contestabile

Received: 12 February 2024
Revised: 3 March 2024
Accepted: 8 March 2024
Published: 10 March 2024

1. Introduction

The basic principle for light confinement and propagation in optical fibers is total internal reflection. Total internal reflection was first studied by Johannes Kepler in 1611 [1]. In 1621, it was mathematically described by Willebrord Snellius (Snell's law), but remained unpublished during his lifetime. In 1690, Christiaan Huygens in his Treatise on Light showed how Snell's law of sines could be explained by the wave nature of light [2]. Optical fibers are one of the major technological successes of the 20th century.

The first uncladded glass fibers were fabricated in the 1920s [3]. In the 1950s, a cladding layer was added [4–6]. The cladding layer considerably improved the fiber characteristics. The early fibers were very lossy (~1000 dB/km). The situation changed in the 1970s when silica fibers with a loss of ~20 dB/km were developed [7]. In 1979, a loss level of ~0.2 dB/km near the 1550 nm wavelength was achieved [8]. It was limited mainly by Rayleigh scattering. Such low-loss fibers have led to a revolution in optical fiber communications and to the advent of nonlinear fiber optics, fiber lasers and amplifiers, and fiber sensors.

Stimulated Raman and Brillouin scattering in optical single-mode fibers were investigated both theoretically and experimentally in 1972 [9–11]. In 1973, it was suggested that optical fibers can support solitons [12]. Almost at the same time, optically induced birefringence, parametric four-wave mixing, and self-phase modulation were observed in optical fibers.

The use of rare earth (RE)-doped optical fibers for gain in glass fiber lasers and amplifiers was first demonstrated by Eli Snitzer in 1961 [13]. He used a neodymium-doped silicate glass fiber emitting at 1060 nm. In the 1990s, erbium-doped fiber amplifiers and lasers were under intensified investigation [14]. These devises were commercialized in 1992 and employed in undersea fiber-optic communication systems by 1995.

The state-of-the-art design of optical fibers is a careful trade-off between optical losses, optical nonlinearity, group–velocity dispersion, and polarization effects.

In 1978, Pochi Yeh and colleagues proposed the idea of a photonic crystal fiber (PCF) [15]. They proposed to clad a fiber core with Bragg grating, which is similar to 1D photonic crystal. In 1992, Philip Russell invented a photonic crystal fiber made of 2D photonic crystal with an air core. In 1996, the first fabricated single-mode PCF was reported at the Optical Fiber Conference (OFC) [16]. Photonic crystals are periodic dielectric structures with the period being less than the wavelength of the light. They affect the motion of photons in the same way as an ionic lattice affects the electrons in semiconductors. PCFs are among the most specialized optical lightguides. For example, PCFs can range from fibers with low levels of nonlinearities supporting high-power pulses to highly nonlinear PCFs for supercontinuum generation.

From a theoretical point of view, an optical fiber with a circular core has no birefringence, such that the polarization of a beam sent through the fiber may not change. In reality, however, a small amount of birefringence is always present in an optical fiber due to external perturbations or manufacturing imperfection. Such birefringence causes random power coupling between two polarization modes (polarization crosstalk) in an optical fiber, which is undesirable in a number of applications. A polarization-maintaining fiber (PMF) with intentionally induced birefringence along the entire fiber length maintains two polarization modes without polarization crosstalk. Larger birefringence better prohibits the polarization mode coupling. Birefringence can be induced by loss in rotational symmetry in the refractive index profile or by the stress distribution known as stress birefringence. The first commercially available PMF was introduced in 1983.

Heat generation in fiber lasers is briefly discussed in Section 2. Sections 3–5 are devoted to the latest achievements in RE-doped fiber lasers, Raman fiber lasers, and Brillouin fiber lasers, respectively. Fiber laser applications are considered in Section 6.

2. Heat Generation in Fiber Lasers

For most lasers, the laser wavelength, λ_L, is longer than the pump wavelength, λ_P, (Stokes shift). This is unavoidable for all optically pumped schemes where one pump photon can generate one laser photon. The energy difference between the pump and laser photons can be estimated using the so-called quantum defect:

$$\eta_q = 1 - \frac{\lambda_P}{\lambda_L} \tag{1}$$

The quantum defect is an unavoidable source of heat generation in lasers. The process of generating coherent radiation through laser action is never 100% effective. The quantum defect causes a substantial part of the pump energy to be converted into phonons instead of photons. Heating due to the quantum defect manifests itself in many ways including transverse-mode instability, thermal lensing, and catastrophic fiber damage.

Heat management is one of the most critical issues for scaling higher output laser powers. Although the very high surface-to-volume ratio and optical guidance have provided tremendous progress in the power scalability of high-power fiber lasers, limitations on the power handling capacity of fiber lasers are now encountered.

Under the steady-state operation $(\partial/\partial t = 0)$, the heat conduction equation in an isotropic medium can be written as follows:

$$\nabla^2 T(r,z) = -\frac{Q(r,z)}{\kappa} \tag{2}$$

where T is the temperature, κ is the thermal conductivity, and Q is the dissipated heat density per unit volume. In the center of the fiber core $(r = 0)$, the following equation

$$\left.\frac{\partial T_{co}}{\partial r}\right|_{r=0} = 0 \tag{3}$$

must be satisfied. Here, r is the fiber radius, and T_{co} is the temperature of the fiber core. The core and cladding temperatures and their derivatives must be continuous across the borders.

$$T_{co}(r_{co}) = T_{cl}(r_{co}) \tag{4}$$

$$\kappa_{co} \left.\frac{\partial T_{co}}{\partial r}\right|_{r=r_{co}} = \kappa_{cl} \left.\frac{\partial T_{cl}}{\partial r}\right|_{r=r_{co}} \tag{5}$$

$$\kappa_{cl} \left.\frac{\partial T_{cl}}{\partial r}\right|_{r=r_{cl}} = h[T_c - T_{cl}(r_{cl})] \tag{6}$$

where T_{cl} is the temperature of the fiber cladding. r_{co} and r_{cl} are the core and cladding radii, respectively. κ_{co} and κ_{cl} are the thermal conductivities of the core and cladding, respectively. h is the heat transfer coefficient. T_c is the environmental temperature. Considering $Q(r,z) \cong Q(z)$ and taking into account the boundary conditions (3)–(6), one can estimate the temperature of the fiber [17].

$$T_{co}(r,z) = T_0(z) - \frac{Q(z)r^2}{4\kappa_{co}}, \text{ if } 0 < r < r_{co} \tag{7}$$

$$T_{cl}(r,z) = T_0(z) - \frac{Q(z)r_{co}^2}{4\kappa_{co}} - \frac{Q(z)r^2}{2\kappa_{cl}} ln\left(\frac{r}{r_{co}}\right), \text{ if } r_{co} < r < r_{cl} \tag{8}$$

$$T_0(z) = T_c + \frac{Q(z)r_{co}^2}{2hc} + \frac{Q(z)r_{co}^2}{4\kappa_{co}} + \frac{Q(z)r_{co}^2}{2\kappa_{cl}} ln\left(\frac{r_{cl}}{r_{co}}\right) \tag{9}$$

Here, T_0 is the temperature at the core center. As seen from (7)–(9), the temperature profiles are significantly affected by pump evolution along the fiber length [17]. The temperature distribution is uneven along the fiber. In the forward pump mode, the maximum temperature is attained at the input side of the laser cavity, which corresponds to the intense amplification of the laser signal, accompanied by a tremendous increase in the number of the phonons ("superfluous" phonons), causing heating of the laser medium [17,18]. In the two-end pump mode, the temperature evolution is more even. Under these conditions, the maximum temperature is attained on both sides of the laser cavity [17,19].

The radial distribution of the temperature profile is more even than the axial distribution. It can be ignored while significant heat is traveling through the axial direction of the fiber [17,19].

Apart from the quantum defect, photodarkening in high-power fiber lasers can also lead to increased background absorption, resulting in excess heating. Photodarkening is color-center formation through some type of structural change in the glass which may or may not be reversible [20,21].

3. Rare Earth-Doped Fiber Lasers

The wide range of industrial and defense applications has fueled the development of RE-doped fiber lasers. Fibers used for data transmission are known as passive fibers, since they do not change the power of the propagating signal. RE-doped fibers can amplify the propagating optical signal. They are called active fibers. The successful development of low-loss optical fibers doped with various RE elements, such as ytterbium (Yb), erbium (Er), thulium (Tm), holmium (Ho), praseodymium (Pr), or dysprosium (Dy), opened the door to creating fiber lasers. Each RE-doped fiber laser has a specific emission window defined by its dopant. For example, Yb^{3+}-doped fiber lasers have a window of emission wavelengths ranging from ~1050 nm to ~1120 nm; Er^{3+}-doped fiber lasers have a window of emission wavelengths ranging from ~1530 nm to ~1590 nm.

A laser beam can be characterized by its brightness:

$$B = \frac{P}{A\Omega} = \frac{P}{(M^2)^2\lambda^2} \tag{10}$$

where P is the source power divided by the product of the mode area, $A = \pi w_0^2$, and the solid angle, $\Omega = \pi\theta_0^2$. Here w_0 and θ_0 are the beam waist and half-angle divergence, respectively. λ is the wavelenght of the laser beam.

$$M^2 = \frac{\pi w_0 \theta_0}{\lambda} \tag{11}$$

Equation (11) is used to calculate the beam quality factor.

3.1. Rare Earth Ions for Laser Applications

RE atoms include Sc, Y, and two groups: lanthanides with atomic numbers 57 through 71 (characterized by filling the 4f shell); and actinides with atomic numbers 89 through 103 (characterized by filling the 5f shell). In solids, the trivalent (3+) level of ionization is the most stable for lanthanide ions. RE ions have the sharp spectral lines. The sharp spectral lines in the optical spectra of trivalent RE ions are a consequence of the screening of 4f valence electrons by the 5s and 6d electrons due to the effects of the environment. An ion in a solid can be considered an impurity (a dopant) embedded in a host material. The ion replaces the host ion and forms an optically active center. The host materials play a fundamental role in the spectral nature of doped ions.

Laser glasses can be divided into oxide, halide, oxyhalide, and chalcogenides [22]. Glasses are amorphous over a long range but contain a local order. Glasses are insulators with bandgaps greater than 5 eV (the deep UV). All transitions in ions occur within the host bandgap. The energy levels of ions typically are identified by three principal quantum numbers: L, S, and J. L describes the total orbital angular momentum, S the total spin angular momentum, and J the total angular momentum. There are several possible ways to obtain a given set of values for L, S, and J. The possible states are referred to by the symbol $^{2S+1}L_J$, where $L = 0, 1, 2, 3, 4, \ldots$ corresponds to letters $S, P, D, F, G \ldots$, respectively. Schematical diagrams of energy levels with transitions for Yb^{3+}, Er^{3+}, Tm^{3+}, and Ho^{3+} ions are presented in Figure 1.

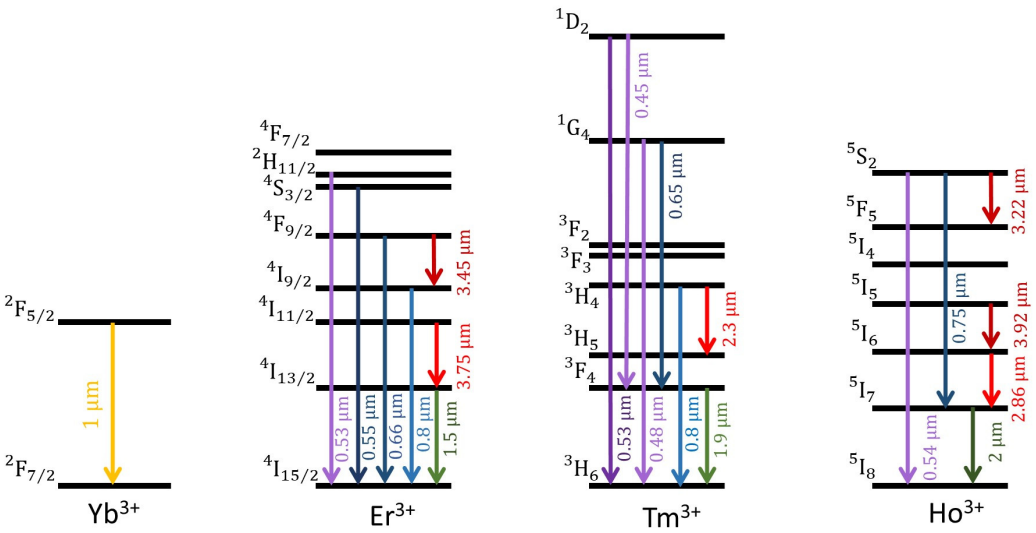

Figure 1. Diagrams of energy levels and transitions for some Yb^{3+}, Er^{3+}, Tm^{3+}, and Ho^{3+} ions.

Several states can correspond to the same atomic energy level (degeneracy). In RE-doped ions, this degeneracy is lifted through interaction with the local environment. Fiber lasers have been realized with a wide variety of RE ions including ytterbium (Yb^{3+}), erbium (Er^{3+}), thulium (Tm^{3+}), holmium (Ho^{3+}), praseodymium (Pr^{3+}), and dysprosium (Dy^{3+}). The most used RE ions for laser applications are Yb^{3+}, Er^{3+}, and Tm^{3+}. As one can see in Figure 1, only Yb^{3+} ions have only one excited state, that is, only Yb^{3+} ions are free from excited state absorption, which can serve as a source of heat generation.

Pump radiation excites electrons from the ground level to higher levels. Excited electrons can undergo spontaneous (radiative or nonradiative) decay or stimulated transition. The spontaneous decay process can be characterized by the lifetime of the excited level τ_{ex} as follows:

$$\frac{1}{\tau_{ex}} = \frac{1}{\tau_r} + \frac{1}{\tau_{nr}} \tag{12}$$

$$\frac{1}{\tau_{nr}} = C\left[\widetilde{n}(T) + 1\right]^p exp(-\alpha \Delta E) \tag{13}$$

where C is an empirical parameter that depends on the host.

$$\widetilde{n}(T) = \left[exp\left(\frac{\hbar\Omega}{\kappa_B T}\right) - 1\right]^{-1}, \quad p = \frac{\Delta E}{\hbar\Omega}, \quad \alpha = -\frac{ln(\varepsilon)}{\hbar\Omega} \tag{14}$$

ΔE is the energy gap, ε is an electron–phonon coupling coefficient, $\hbar\Omega$ is the maximum phonon energy of the host, $\hbar$ is the reduced Planck constant, T is the temperature of the host, κ_B is the Boltzmann constant, and p is the number of phonons required to bridge the ΔE gap. The empirical parameters of relation (13) for some host materials can be found in [23–25]. The spontaneous decay process can be characterized by the mean fluorescence wavelength, λ_F, or the mean fluorescence frequency, ω_F.

$$\lambda_F = \frac{2\pi c}{\omega_F} = \frac{\int \lambda I_F(\lambda) d\lambda}{\int I_F(\lambda) d\lambda} \tag{15}$$

where c is the speed of light in the vacuum, and $I_F(\lambda)$ is the fluorescence intensity at the wavelength λ.

If the upper level is more populated than the lower level, a population inversion takes place in the system. Population inversion is a necessary condition for amplification or lasing. It is impossible to attain population inversion in a two-level system [26]. The system must have at least three levels in order to be suitable for laser amplification. A commonly used four-level laser scheme is presented in Figure 2a for Yb^{3+} ions. In this scheme, two levels of the ground manifold and two levels of the excited manifold are involved in a laser cycle.

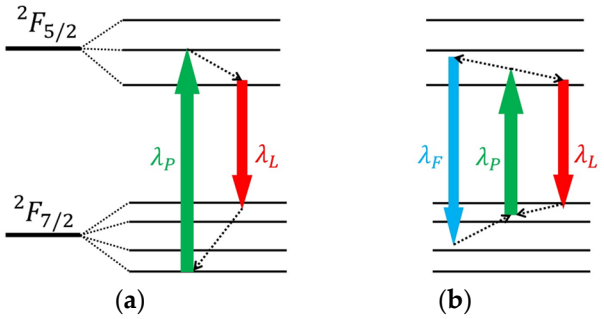

Figure 2. Energy diagrams of a traditional four-level laser (**a**) and a radiation-balanced laser (**b**). λ_P and λ_L are the pump and laser frequencies, respectively. λ_F is the mean fluorescence frequency. Solid and dushed arrows illustrate photon and phonon transitions, respectively.

As mentioned above, the quantum defect, η_q, is an unavoidable source of heat generation in lasers. The heat generation process is responsible for transverse-mode instability, thermal lensing, and catastrophic fiber damage. In RE-doped fiber lasers, heating can also cause a reduction in both the emission and absorption cross-sections of the RE ions, affecting the gain of the active fiber. Once the concentration of the RE ions exceeds a certain limit, cooperative effects such as an energy transfer process, a cross-relaxation process, nonradiative energy transfer, cooperative emission, and excitation become essential. Some of these processes can cause heat generation [27]. Cooperative effects limit the maximum

ion concentration that can be doped into the fiber, resulting in the use of longer fibers. On the other hand, a longer fiber can serve as a source of nonlinear effects, for example, Raman and Brillouin scattering.

3.2. RE-Doped Radiation-Balanced Fiber Lasers

In 1999, Steven Bowman [28] proposed a radiation-balanced (athermal) RE-doped laser which operates without internal heating. In this laser, all photons generated in the laser cycle are annihilated in the cooling cycle, that is, the heat generated from the stimulated emission is offset by cooling from anti-Stokes emission (Figure 2b). The idea of optical cooling using anti-Stokes fluorescence was first proposed by Pringsheim in 1929 [29]. It is significant that in order to keep the radiation balance at each point in the laser medium, the pump intensity must be distributed properly along the length of the laser fiber. Any deviation from this distribution will result in heating or cooling in some parts of the laser medium. In radiation-balanced lasers and amplifiers, the power of the amplified signal increases only linearly with the length of the active medium. The theory of radiation-balanced (athermal) RE-doped fiber amplifiers was developed in [30]. To overcome the problem of linear signal power growth, fiber lasers and amplifiers with a cooler made from RE ions and integrated into the body of the device have been proposed and theoretically investigated [18,31,32]. The theory of mJ-level pulse amplifiers in Yb-doped double-clad optical fibers was developed in ref. [33].

In 2021, the first radiation-balanced silica fiber amplifier was demonstrated. An Yb^{3+}-doped silica fiber served as an active medium [34]. The core diameter of the silica fiber was 21 μm. Its numerical aperture was 0.13. The Yb^{3+} concentration was 2.52 wt.%. The fiber was co-doped with 2.00 wt.% Al to reduce concentration quenching. The wavelength of the pump was 1040 nm and the signal wavelength was 1064 nm. The mean fluorescence wavelength of Yb^{3+} was 1003.9 nm and the radiative and quenching lifetimes were 765 μs and 38 ms, respectively. The Yb^{3+} critical quenching concentration was 21.0 wt.%. The absorptive loss of the fiber was 18 dB/km. The temperature of the fiber decreased to ~130 mK below room temperature. Different schemes of athermal lasers and amplifiers are overviewed in ref. [35]. The latest advances in radiation-balanced fiber lasers and amplifiers are considered in ref. [36].

3.3. Power Evolution of RE-Doped Fiber Lasers

The rapid development of active RE-doped optical fibers has led to the development of high-power lasers with output powers of tens or hundreds of watts, sometimes even several kilowatts, from a single fiber. High-power laser sources are widely used in industrial precision processing. They can serve as a new platform for strong-field physics research using peak power over petawatt.

As noted above, Yb^{3+} ions are widely used in fiber lasers. Since they have only two manifolds, they are free from a number of cooperative effects. The quantum efficiency of Yb^{3+}-doped fiber lasers is close to 100% due to the low energy difference between the pump and laser photons. The Yb^{3+} ions possess a broadband absorption spectrum ranging from ~850 nm to ~1080 nm, with the peak in the range between ~915 nm and ~980 nm. The window of emission wavelengths from Yb^{3+}-doped fiber lasers is limited to a small band (1050–1160 nm). At this junction, all-fiber laser oscillators operating at ~1000 nm are well developed. Their power evolution throughout the past several years is presented in Figure 3 [37–48].

As can be seen in Figure 3, the maximum power ~8.5 kW was reached in 2020. Fiber lasers with wavelengths of 980 nm, 1007 nm, 1018 nm, and 1150 nm have attracted significant interest since they are very useful in nonlinear frequency conversion and efficient pumping of other RE-doped fibers which have absorption bands located near these wavelengths. A 1.3 kW, 1018 nm fiber laser with a beam quality M^2 less than 1.1 was reported by IPG Photonics [49].

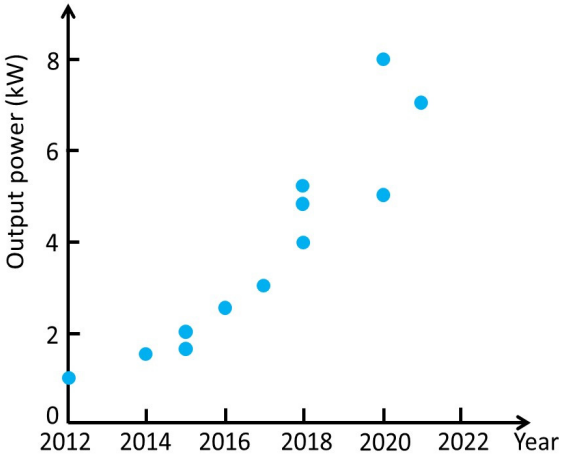

Figure 3. Power evolution of all-fiber laser oscillators operating at ~1000 nm [37–48].

The Er^{3+}-doped and Er^{3+}-Yb^{3+} co-doped fiber lasers partly complement the emission range of 1530–1590 nm. The power evolution of these fiber lasers at ~1500 nm throughout the past several years is presented in Figure 4 [50–61]. The highest power achieved with Er^{3+}-doped fibers with a relatively multimode operation (M^2 ~ 10.5) is 656 W [56].

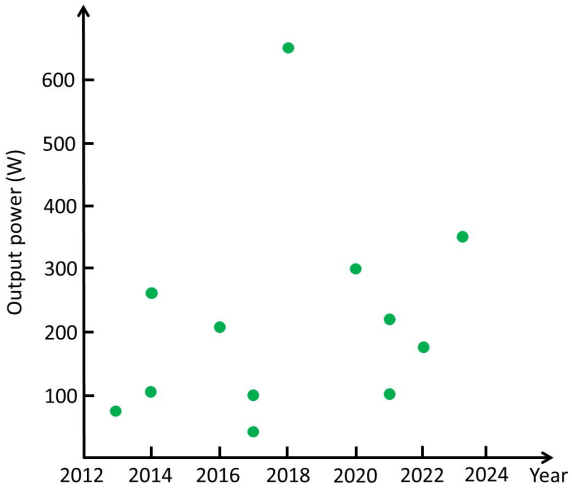

Figure 4. Power evolution of Er^{3+}-doped and Er^{3+}-Yb^{3+} co-doped fiber lasers operating at ~1.5 μm [50–61].

The Tm^{3+}-doped and Tm^{3+}-Ho^{3+} co-doped fiber lasers have an emission range between ~1900 nm and ~2100 nm. The output power ~1.2 kW at ~2000 nm was obtained with these lasers in 2018. Their power evolution is presented in Figure 5 [62–71].

Recent experiments have demonstrated the single-mode Ho-doped fiber laser providing 407 W of output power [72].

The Er^{3+}- and Tm^{3+}-doped lasers are significantly limited in power and efficiency compared to Yb^{3+}-doped fiber lasers. As one can see in Figures 4 and 5, the erbium lasers are limited to a few hundred watts; the thulium lasers have achieved power levels of around a kilowatt. Greater quantum defects, difficulty in increasing the ion concentration, excited state absorption, and cooperative effects prevent the erbium and thulium dopants from competing in the output power with ytterbium.

Although fiber laser systems exceeding 100 kW are commercially available [73], there is still a lot of room for further development of the RE-doped fiber lasers with excellent optical properties.

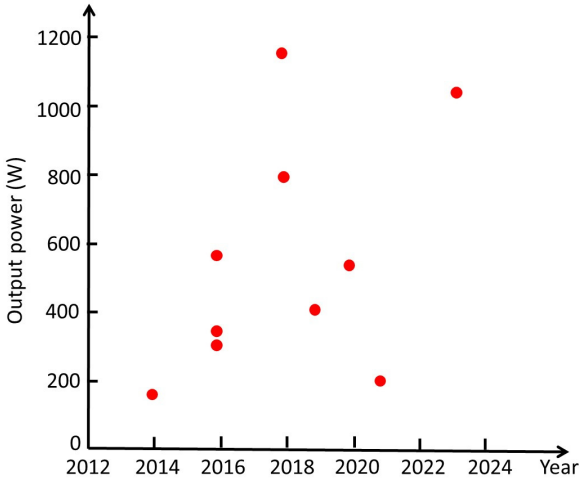

Figure 5. Power evolution of Tm^{3+}-doped and Tm^{3+}-Ho^{3+} co-doped fiber lasers operating at ~2 μm [62–71].

4. Raman Fiber Lasers

There are substantial white spaces in the wavelength spectrum where no RE-doped fiber lasers are available. Raman fiber lasers can cover these white spaces. In contrast to RE-doped lasers, Raman lasers are free from photodarkening.

4.1. Heat Mitigation in Raman Fiber Lasers

In 1963, Charles Townes introduced the concept of stimulated Raman scattering (SRS) [74]. In ref. [74], it has been shown that since the laser light incident on a medium is coherent, the resulting emission occurs through a parametric process due to the interaction between the coherent molecular oscillations (optical phonons) and the coherent laser light.

The lasing mechanism of Raman lasers is based on stimulated Stokes Raman scattering (SSRS) in a Raman medium (Figure 6a). An incoming pump photon with the energy $\hbar\omega_P$ scatters into a lower-energy Stokes photon $\hbar\omega_S$ and a phonon with the energy $\hbar\Omega_{op}$, which serves as a source of heat generation. As can be seen in Figure 6a, Raman lasers, like RE-doped lasers, suffer from heat dissipation inside the active medium caused by the quantum defect between the pump and lasing (Stokes) photons. Like in the case of RE-doped lasers, heat generation in Raman lasers can degrade their performance. Heat mitigation in Raman lasers can be achieved in different ways.

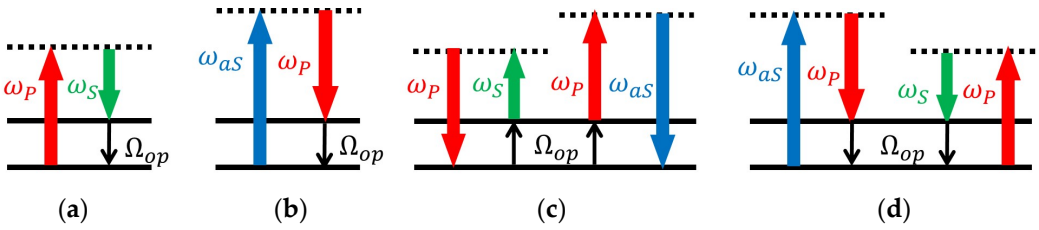

Figure 6. Processes that take place in a Raman laser: (**a**) stimulated Stokes Raman scattering (SSRS), (**b**) stimulated anti-Stokes Raman scattering (SARS), (**c**) coherent anti-Stokes Raman scattering (CARS) when it converts a Stokes photon and a pump photon to an anti-Stokes photon and a pump photon, annihilating two phonons, and (**d**) CARS when it converts an anti-Stokes photon and a pump photon to a Stokes photon and a pump photon, creating two phonons. ω_P, ω_S, ω_{aS}, and Ω_{op} are the pump, Stokes, anti-Stokes, and optical phonon frequencies, respectively.

One way to mitigate heat dissipation in Raman lasers has been proposed in [75–77]. It relies on three different Raman processes that can occur inside the medium of an optically pumped Raman laser illustrated in Figure 6. Besides SSRS, stimulated anti-Stokes Raman scattering (SARS) and coherent anti-Stokes Raman scattering (CARS) can take place in the

Raman medium. The maximum Raman gain point is considered in Figure 6, that is, all scattering processes are exactly at the Raman resonance. As stated above, the SSRS, which is responsible for lasing, is a source of heat generation. In common with SSRS, the SARS process generates quantum-defect heating too. In this process, an anti-Stokes photon is converted into a pump photon and a phonon (Figure 6b). CARS at the Raman resonance presented in Figure 6c is a four-wave mixing process. It converts a pump photon and a Stokes photon into a pump photon and an anti-Stokes photon, annihilating two phonons responsible for heating [78]. This process reduces the quantum-defect heating in the Raman medium. Phase matching is very important in this scheme. If it is not satisfied, the induced phase variation along the propagation direction of the amplified signal will cause the CARS process to alternate, reversing periodically at the coherence length (Figure 6c,d). This approach to Raman processes, which was developed by Bobbs and Warner in ref. [78], is different from the traditional one, where the CARS is seen as a mechanism that converts two pump photons into Stokes and anti-Stokes photons without exchanging energy with the Raman medium. By this means, the intrinsic heat-mitigation technique in Raman lasers relies on CARS (Figure 6c) instead of anti-Stokes fluorescence.

The harnessing of frequency-selective dissipative coupling to reduce the heat generated by CARS reversed cycles in active Raman media with phase mismatching was proposed in ref. [79] for waveguide systems. This approach can be applied to a fiber Raman system too. Heat mitigation in this approach is accomplished using a coupled waveguide structure, which includes the active Raman waveguide (RW), where the Stokes signal undergoes amplification via SSRS, and a dissipative waveguide (DW), which is tuned to the anti-Stokes wavelength so as to evacuate the corresponding anti-Stokes photons from the RW by coupling. The DW introduces optical loss that partially offsets the growth of the anti-Stokes signal in the RW and hence suppresses the reversed CARS cycles that would otherwise result in heat generation in the RW. It is shown that the frequency-selective dissipative coupling provided by the DW can reduce the heat in active Raman media by a factor of up to five when the CARS phase mismatch is compensated for by the optimum level of coupling between the RW and the DW.

The alternative approach to mitigating heat dissipation in Raman lasers is based on an ultralow quantum defect. In the majority of cases, high-power Raman fiber lasers are made of pure silica fibers or germanium-doped fibers. The lowest quantum defect for such a Raman laser pumped at 1064 nm and emitted at 1075 nm is 1.02% [80]. The pump power of the laser is 6.5 W and the output power is 1.1 W. It is difficult to achieve a high-power Raman output with such a low quantum defect, because the Raman gain in the pure silica fiber or germanium-doped fiber is relatively low at such a small frequency shift.

In 2020, the phosphosilicate-doped passive fiber was proposed for low quantum defect applications [81]. This fiber has a strong boson peak and a Raman gain peak at a frequency shift of ~40 THz in its Raman gain spectrum. The Raman gain peak is related to the asymmetric stretching vibrations supported by phosphorus–oxygen double bonds. This peak has been used for high power generation in Raman fiber lasers [82]. The boson peak in the phosphosilicate fiber is ascribed to an excess density of vibrational states [83]. In ref. [81], an ultralow quantum defect Raman laser based on the boson peak in phosphosilicate fibers has been reported for the first time. In this laser, the amplification process is based on a strong boson peak located at a frequency shift of 3.65 THz in its Raman gain spectrum. At a pump wavelength of 1066 nm and a pump power of 18.6 W, the Stokes output at the wavelength 1080 nm has reached 12.5 W. The quantum defect is 1.3%. For the increased pump wavelength, 1072 nm, the output power at 1080 nm is 10.7 W. In this case, the quantum defect is 0.74%. This is the lowest quantum defect ever reported for Raman fiber lasers.

4.2. Brightness Enhancement in Raman Fiber Lasers

In cladding-pumped RE-doped fiber lasers, the low-brightness pump light is coupled into the fiber cladding while the laser signal undergoes amplification in a fiber core, which

supports only low-order modes with superior brightness relative to the pump. Brightness enhancement in the system can be estimated as follows:

$$BE = B_L / B_P \tag{16}$$

where B_L and B_P are the laser output brightness and the pump input brightness, respectively. Like RE-doped fiber lasers, Raman fiber lasers can provide brightness enhancement too. For example, one can use the same cladding-pumped approach (usually based on double cladding) to achieve brightness enhancement in Raman lasers.

Another way to achieve brightness enhancement in Raman fiber lasers consists of utilizing multimode graded-index (MM-GRIN) fibers. As in the case of the cladding-pumped approach, in the MM-GRIN approach, the Stokes laser signal is generated in the high-brightness core, while the pump propagates through a larger diameter of the fiber cladding. The first Raman fiber laser based on MM-GRIN fibers was demonstrated in 2018 [84]. A total of 135 W of the output power was obtained with 68% efficiency relative to launched pump power. Its brightness enhancement was $BE \approx 5.6$.

Much progress has been made in the last few years in both of these techniques. In 2018, the highest brightness enhancement $BE \approx 7$ for the cladding-pumped configuration was demonstrated at a record Raman fiber laser power of 1.2 kW with 85% efficiency relative to launched pump power [85]. At such high (over kW) output power levels, the beam quality $M^2 \approx 2.75$ was obtained.

In 2019, a Raman fiber laser power of 1002.3 W at 1060 nm with 84% efficiency was demonstrated using the MM-GRIN configuration [86]. The brightness enhancement was about 2.57 at the maximum output power. The beam quality was $M^2 \approx 5$.

5. Brillouin Fiber Lasers

Brillouin scattering is the interaction of optical waves with acoustic waves in a medium. It was described by Leon Brillouin in 1922 [87], and independently by Leonid Mandelstam in 1926 [88]. In the 1960s, Charles Townes, who introduced SRS in 1963, realized that parametric interactions could also occur between laser light and the acoustic branch of the phonon spectrum, that is, between laser light and acoustic oscillations (acoustic phonons), or sound waves. This process is known as stimulated Brillouin scattering (SBS). The first demonstration of SBS was reported in 1964 in quartz and sapphire crystals [89]. As a third-order nonlinear optical process, SBS requires intense radiation. Compared to typical Raman frequency shifts (50–1400 cm^{-1}), the Brillouin frequency shift (0.1–2 cm^{-1}) is extremely small. Brillouin scattering (both stimulated and spontaneous) manifests itself through the generation of backward or forward propagating waves shifted from the frequency of the incident pump wave by an amount determined by the frequency of the acoustic phonon. When the acoustic wave is moving away from the pump light beam, the Stokes shift takes place in the system (Figure 7a). When the acoustic wave is moving toward the pump light beam, the anti-Stokes shift takes place (Figure 7b).

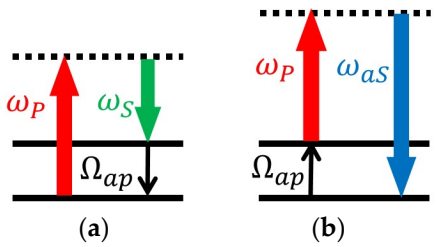

Figure 7. The energy level diagram of Brillouin scattering. (**a**) Brillouin Stokes scattering; (**b**) Brillouin anti-Stokes scattering. ω_P, ω_S, ω_{aS}, and Ω_{ap} are the pump, Stokes, anti-Stokes, and acoustic phonon frequencies, respectively.

The energy and momentum conservation requirements of Stokes and anti-Stokes Brillouin scattering have the forms

$$\omega_S = \omega_P - \Omega_{ap} \quad \text{and} \quad \boldsymbol{k_S} = \boldsymbol{k_P} - \boldsymbol{K_{ap}} \tag{17}$$

for Stokes scattering and

$$\omega_{aS} = \omega_P + \Omega_{ap} \quad \text{and} \quad \boldsymbol{k_{aS}} = \boldsymbol{k_P} - \boldsymbol{K_{ap}} \tag{18}$$

for anti-Stokes scattering. Here ω_P, ω_S, and ω_{aS} are the pump, Stokes, and anti-Stokes photon frequencies, respectively. Ω_{ap} is the acoustic wave frequency. $\boldsymbol{k_P}$, $\boldsymbol{k_S}$, $\boldsymbol{k_{aS}}$, and $\boldsymbol{K_{ap}}$ are the pump, Stokes, anti-Stokes, and acoustic phonon wave vectors, respectively. In the SBS process, $\Omega_{ap} \ll \omega_P$, ω_S, ω_{aS}. As for Raman scattering, the Stokes scattering process is accompanied by phonon generation (heating); the anti-Stokes scattering process is accompanied by phonon absorption (cooling).

SBS can be used for the development of Brillouin lasers. A typical Brillouin laser involves coupling a laser pump light source, whose spectral width is much less than the Brillouin gain bandwidth, to the optical fiber in order to produce SBS with the Stokes signal propagating in the backscattered path of the incident pump light. The first Brillouin fiber laser was presented in 1976 [90]. Since then, remarkable progress in the development of Brillouin fiber lasers has been made. Great effort went into the development of lasers with a relatively low pump threshold, high efficiency, small linewidth, and especially multiwavelength configurations.

Multiwavelength Fiber Lasers

SBS is the most attractive technique for the development of multiwavelength fiber lasers, which have the advantages of a narrow linewidth, low-intensity noise, stable operation at room temperature, and potential applications in optical communication, optical sensors, gas spectroscopy, and microwave photonics.

The cascaded SBS process occurs when the power of the first-order Stokes signal reaches the SBS generation threshold of the second-order Stokes (Figure 8). The first-order anti-Stokes signal can also be generated due to the four-wave mixing process between the pump and the first-order Stokes wave. The typical frequency shift in the Brillouin spectrum in most glass is about ~10 GHz. This narrow frequency shift is a challenge for the demultiplexing and signal filtering processes in optical communication applications. Several approaches have been developed to increase the frequency spacing range and to reduce the complexity of demultiplexing. These approaches include widely used double Brillouin frequency spacing of 0.17 nm [91–93] and a triple Stokes line spacing of 0.25 nm [94–97]. A quintuple wavelength spacing of 0.4 nm was presented in ref. [98], where four quintuple Brillouin Stokes signals with a high Stokes power of 10 dBm and a signal-to-noise ratio of 50 dB were achieved. The recorded Stokes signals were tuned over a wavelength range of 40 nm (1540–1580 nm).

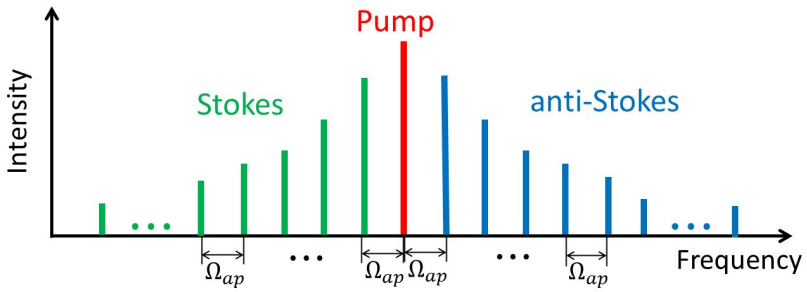

Figure 8. Illustration of the cascaded SBS process. It occurs via the interplay of SBS and four-wave mixing.

The sextuple Stokes signal 0.48 nm has been demonstrated in ref. [99], utilizing a triple unidirectional ring laser cavity. Three sextuple channels are achieved and tuned over a wavelength range of 15 nm (1560–1575 nm). In this work, up to three sextuple Stokes lines with a high signal power of 10 dBm and a large optical signal-to-noise ratio of more than 55 dB have been demonstrated. It has been shown that the generated Stokes lines can be tuned over a wavelength range of 15 nm from 1560 to 1575 nm.

A switchable multiwavelength Brillouin fiber laser has been proposed and demonstrated with channel spacing from 10 GHz up to even more than 100 GHz at a step of 10 GHz [100]. The structure comprises two nonlinear fiber loops, a feedback path, and a tunable optical bandpass filter for switchable operation. The multiwavelength Brillouin fiber laser is generated in the nonlinear fiber loop, where a dual-pump source produces dual Brillouin lasers that give rise to a wideband multiwavelength Brillouin fiber laser via the four-wave mixing effect. Some achievements of multiwavelength Brillouin fiber lasers across different spectral regions have been discussed in ref. [101].

Fiber lasers based on backward SBS have been studied and employed for over thirty years. As mentioned, SBS in fibers takes place in the forward direction as well, with amplification bandwidths which are narrower by two orders of magnitude. The first forward Brillouin fiber laser, using a bare off-the-shelf, panda-type PMF, has been reported in ref. [102]. Pump light in one principal axis provides Brillouin amplification for a co-propagating lasing signal of the orthogonal polarization. Feedback is provided by Bragg gratings at both ends of the optical fiber cavity. Single-mode, few-mode, and multimode regimes of operation have been observed. A laser threshold has been observed at a pump power level of 26.5 dBm. The output power of the laser was saturated at 250 μW due to the onset of backward SBS in the fiber cavity. The differential slope efficiency of the laser output power between the threshold and saturation was approximately 0.005. Forward SBS fiber lasers are extremely sensitive to changes in media outside the cladding. They can serve as highly coherent laser sources and ultraprecision forward SBS sensors.

6. Fiber Laser Applications

At present, fiber lasers are used widely in both science and industry. As mentioned above, in the 1990s, fiber lasers came into wide use in the realm of the telecommunications industry, providing high-quality single-mode low-power systems. Fiber lasers in fiber telecommunications are mainly used as light sources. Since fiber lasers have the characteristics of high efficiency, stability, and good modulation performance, they can provide stable and high-quality optical signals.

With the collapse of the telecommunications markets in the early 2000s, fiber laser producers shifted their focus to meeting the needs of industrial material processing, and of military and medical sectors. This shift to alternative markets required higher-power lasers. One particular advantage of fiber lasers is that they are inherently simple and can therefore provide easily manufacturable systems to meet a range of power levels and output quality.

6.1. Material Processing

The application of fiber lasers in the field of material processing mainly includes laser cutting, laser welding, and laser marking. High-speed and high-precision material processing can be achieved using high-power and high-beam-quality fiber lasers.

The use of fiber lasers has allowed, for the first time, for the generation of striation-free cuts in the case of oxygen-assisted laser cutting of 1 mm and 2 mm thick mild steel sheets [103]. Nowadays, fiber laser flexibility enables the cutting of a wide range of materials from steel and aluminum to nonmetal materials such as plastics and glass of different thicknesses. The fiber laser cutting process results in a high-quality cutting edge. High-power CW fiber lasers are commonly used for industrial applications. As the power output increases, the cutting speed and the ability to process thicker materials improve, making them ideal for high-volume production.

The excellent mode quality and high focusability of low-power single-mode fiber lasers are the most important features for achieving small spot sizes in the range of some microns. As a result, the welding of microparts with very high processing speeds, the lowest energy input, reduced heat-affected zones, and minimized distortion has been achieved [104]. At present, fiber laser welding creates strong welds and good-quality joints, even with dissimilar materials. With the benefit of consistent accuracy, laser welding is well suited to manufacturing processes with repetitive operations. Fiber lasers are also very useful in microprecision welding and laser spot welds.

Fiber lasers are perfect for laser marking. Laser marking is a process in which a laser beam is used to mark or engrave a surface at a high speed and low-operating cost.

6.2. Military Sector

Fiber lasers have high temperature and high corrosion resistance, which is especially suitable for military applications. Fiber lasers can serve as one of the main light sources of tactical laser weapons [105]. In fiber optic radar, fiber lasers can be used as laser sources to provide high-power and high-stability laser signals for target detection and tracking.

6.3. Medical Sector

With the continuous progress of science and technology, fiber lasers are increasingly widely used in laser therapy [106]. Laser energy can be delivered through optical fibers to accurately treat diseased tissues. In laser therapy, fiber lasers have the advantages of high energy density, high orientation, and minimally invasive treatment. The application of fiber lasers in laser therapy includes but is not limited to laser beauty treatment, laser eye therapy, laser tumor therapy, and laser endoscopic therapy.

6.4. Optical Frequency Combs

The invention of optical frequency combs (OFCs), also known as the rulers of light, has enabled numerous applications in the fields of optical metrology, spectroscopy, astronomy, and quantum and attosecond science [107].

Over the past two decades, various types of OFC sources have been demonstrated, including solid-state or fiber-based mode-locked combs, electro-optic combs, and microresonator-based combs. At present, mode-locked fiber combs are technically mature and have a deeper degree of commercialization. This is due to their low noise performance and long-term reliability. OFCs can be realized utilizing various mode-locking techniques, such as nonlinear polarization rotation, a real saturable absorber, and a nonlinear amplifying loop mirror. Fiber laser-based OFCs are particularly attractive for free-space time–frequency transfer, low-noise microwave generation, and gas molecule detection.

6.5. Quantum Applications

Quantum optics is based on lasers as light sources. Fiber lasers can be used as pump sources in single-photon emitters and in waveguide quantum electrodynamics [108]. Fiber lasers are actively engaged in the manipulation and readout of quantum bits. They are used widely in the trapping and cooling of atoms and ions as well as in quantum sensing and metrology.

7. Conclusions

The present work gives a brief overview of the latest achievements in fiber lasers including RE-doped fiber lasers, Raman fiber lasers, and Brillouin fiber lasers. In comparison to conventional bulk lasers, fiber lasers have a number of advantages.

- The inherently flexible structure of fibers enables the use of much longer (up to several kilometers) gain distances, which provides higher optical gains, compared to other lasers.
- The optical feedback in fiber lasers is usually provided by fiber Bragg gratings imprinted in the fiber. This integrated design provides a stable optical cavity.

- In fiber lasers, single-mode fibers typically offer the best beam performance, which is very important in a number of applications.
- In fiber lasers, the optical path is enclosed within protective cladding layers, and as a result, the laser beam is less susceptible to exterior disturbance compared to traditional lasers.

It has been shown that the Er^{3+}- and Tm^{3+}-doped lasers are significantly limited in power and efficiency compared to Yb^{3+}-doped fiber lasers, which can reach output powers of tens or hundreds of watts. Heat generation in traditional high-power fiber lasers is a serious problem.

- One solution to the heat generation problem is the development of radiation-balanced lasers based on cooling with anti-Stokes fluorescence. The efficiency of the laser cooling process can be improved by applying novel low-phonon fiber materials. The recent achievements in implementing new materials in high-power fiber lasers have been presented in ref. [109], where adverse interactions between the laser light and the host are discussed, and novel composition glass fiber designs and fabrication methodologies are presented.
- The alternative approach to mitigating heat dissipation in Raman lasers is based on an ultralow quantum defect.

As of now, the development of multiwavelength Brillouin fiber lasers with an increased number of Stokes channels that present high flatness and reasonable optical-to-signal ratio is a challenge that fiber laser technology still faces. Multiwavelength Brillouin fiber lasers operating at optical communication wavebands such as 1.5 μm have been widely reported. However, there is still a lot of room for further development of multiwavelength Brillouin fiber lasers in the 1.0 μm, 1.3 μm, and 2.0 μm spectral regions. In these spectral regions, multiwavelength Brillouin fiber lasers show a low optical-to-signal ratio and poor flatness. Finding the best setup parameters for such lasers can considerably improve their performance in these promising spectral ranges.

Although fiber lasers have already revolutionized the laser industry, they continue to be a very promising technique for different applications, including industrial material processing, in military and medical sectors, and quantum physics. Considerable room remains for their improvement.

- As already noted, the optimization of fiber materials is very important for the future development of high-power lasers. The absorption and radiation characteristics of fiber materials can be improved.
- Widely used pump technology such as laser diode pumps and fiber laser pumps can be improved in terms of pump efficiency and fiber absorption efficiency.
- The optical design of fiber lasers can be improved too. For example, specially designed fibers can be developed to achieve brightness enhancement in Raman lasers.

Funding: This research received no external funding.

Institutional Review Board Statement: Not applicable.

Informed Consent Statement: Not applicable.

Data Availability Statement: Not applicable.

Conflicts of Interest: The author declares no conflicts of interests.

References

1. Kepler, J. *Dioptrice*; Prague, Czech Republic, 1611.
2. Huygens, C. *Traité de la Lumière*; Gressner & Schramm: Leipzig, Germany, 1690.
3. Baid, J.L. An improved method of and means for producing optical images. *Br. Pat.* **1927**, *285*, 738.
4. van Heel, A.C.S. A new method of transporting optical images without aberrations. *Nature* **1954**, *173*, 39. [CrossRef]
5. Hirschowitz, B.I.; Curtiss, L.E.; Peters, C.W.; Pollard, H.M. Demonstration of a new gastroscope, the fiberscope. *Gastroenterology* **1958**, *35*, 50–53. [CrossRef] [PubMed]

6. Kapany, N.S. Fiber Optics. VI. Image Quality and Optical Insulation. *J. Opt. Soc. Am.* **1959**, *49*, 779–787. [CrossRef]
7. Kao, K.C.; Hockham, G.A. Dielectric-fibre surface waveguides for optical frequencies. *Proc. Inst. Electr. Eng.* **1966**, *133*, 1151–1158. [CrossRef]
8. Miya, T.; Terunuma, Y.; Hosaka, T.; Miyashita, T. Ultimate low-loss single-mode fibre at l.55 μm. *Electron. Lett.* **1979**, *15*, 106–108. [CrossRef]
9. Stolen, R.H.; Ippen, E.P.; Tynes, A.R. Raman oscillation in glass optical waveguide. *Appl. Phys. Lett.* **1972**, *20*, 62–64. [CrossRef]
10. Ippen, E.P.; Stolen, R.H. Stimulated Brillouin scattering in optical fibers. *Appl. Phys. Lett.* **1972**, *21*, 539–541. [CrossRef]
11. Smith, R.G. Optical power handling capacity of low loss optical fibers as determined by stimulated Raman and Brillouin scattering. *Appl. Opt.* **1972**, *11*, 2489–2494. [CrossRef]
12. Hasegawa, A.; Tappert, F. Transmission of Stationary Nonlinear Optical Pulses in Dispersive Dielectric Fibers. I. Anomalous Dispersion. *Appl. Phys. Lett.* **1973**, *23*, 142–144. [CrossRef]
13. Snitzer, E. Optical maser action of Nd^{3+} in a barium crown glass. *Phys. Rev. Lett.* **1961**, *7*, 444–446. [CrossRef]
14. Desurvire, E. *Erbium-Doped Fiber Amplifiers: Principles and Applications*; John Wiley & Sons, Inc.: Hoboken, NJ, USA, 1994.
15. Yeh, P.; Yariv, A.; Marom, E. Theory of Bragg fiber. *J. Opt. Soc. Am.* **1978**, *68*, 1196–1201. [CrossRef]
16. Knight, J.C.; Birks, T.A.; Russell, P.S.J.; Atkin, D.M. All-silica single-mode optical fiber with photonic crystal cladding. *Opt. Lett.* **1996**, *21*, 1547–1549. [CrossRef]
17. Li, J.; Duan, K.; Wang, Y.; Cao, X.; Zhao, W.; Guo, Y.; Lin, X. Theoretical analysis of the heat dissipation mechanism in Yb^{3+}-doped double-clad fiber lasers. *J. Mod. Opt.* **2008**, *55*, 459–471. [CrossRef]
18. Nemova, G.; Kashyap, R. High-power fiber lasers with integrated rare-earth optical cooler. In Proceedings of the SPIE Laser Refrigeration of Solids III, San Francisco, CA, USA, 23–28 January 2010; Volume 7614, pp. 761406–761416.
19. Chen, Y.; Yao, T.; Xiao, H.; Leng, J.; Zhou, P. Theoretical analysis of heat distribution in Raman fiber lasers and amplifiers employing pure passive fiber. *IEEE Photonics J.* **2020**, *12*, 1504713. [CrossRef]
20. Broer, M.M.; Krol, D.M.; Di Giovanni, D.J. Highly nonlinear near-resonant photodarkening in a thulium-doped aluminosilicate glass fiber. *Opt. Lett.* **1993**, *18*, 799–801. [CrossRef] [PubMed]
21. Atkins, G.R.; Carter, A.L.G. Photodarkening in Tb^{3+}-doped phosphosilicate and germanosilicate optical fibers. *Opt. Lett.* **1994**, *19*, 874–876. [CrossRef] [PubMed]
22. Weber, M.J. Science and technology of laser glass. *J. Non-Cryst. Solids* **1990**, *123*, 208–222. [CrossRef]
23. Layne, C.B.; Lowdermilk, W.H.; Weber, M. Multiphonon relaxation of rare-earth ions in oxide glasses. *J. Phys. Rev. B* **1977**, *16*, 10–20. [CrossRef]
24. Reisfeld, R.; Boehm, L.; Spector, N. Multiphonon relaxation rates and fluorescence lifetimes for Tm^{3+} in four oxide glasses. *Chem. Phys. Lett.* **1977**, *49*, 251–254. [CrossRef]
25. Reisfeld, R.; Jørgensen, C.K. Excited state phenomena in vitreous materials. In *Handbook on the Physics and Chemistry of Rare Earths*; Gschneidner, K.A., Jr., Eyring, L., Eds.; Elsevier: Amsterdam, The Netherlands, 1987.
26. Nemova, G. *Field Guide to Light-Matter Interaction*; SPIE Press: Bellingham, WA, USA, 2022.
27. Nemova, G. *Field Guide to Laser Cooling Methods*; SPIE Press: Bellingham, WA, USA, 2019.
28. Bowman, S.R. Laser without internal heat generation. *IEEE J. Quantum Electron.* **1999**, *35*, 115–122. [CrossRef]
29. Pringsheim, P. Zwei Bemerkungen über den Unterschied von Lumineszenz- und Temperaturstrahlung. *Z. Phys.* **1929**, *57*, 739–746. [CrossRef]
30. Nemova, G.; Kashyap, R. Athermal continuous-wave fiber amplifier. *Opt. Commun.* **2009**, *282*, 2571–2575. [CrossRef]
31. Nemova, G.; Kashyap, R. Fiber amplifier with integrated optical cooler. *J. Opt. Soc. Am. B* **2009**, *26*, 2237–2241. [CrossRef]
32. Nemova, G.; Kashyap, R. Raman fiber amplifier with integrated cooler. *IEEE J. Light. Technol.* **2009**, *27*, 5597–5601. [CrossRef]
33. Yu, N.; Xiong, M.; Dragic, P.D. FDTD modeling of excitation-balanced, mJ-level pulse amplifiers in Yb-doped double-clad optical fibers. *Opt. Express* **2023**, *31*, 32404–32421. [CrossRef]
34. Knall, J.M.; Engholm, M.; Boilard, T.; Bernier, M.; Digonnet, M.J.F. A radiation-balanced silica fiber amplifier. *Phys. Rev. Lett.* **2021**, *127*, 013903. [CrossRef]
35. Nemova, G.; Kashyap, R. Laser cooling of solids. *Rep. Prog. Phys.* **2010**, *73*, 086501. [CrossRef]
36. Nemova, G. Radiation-Balanced Lasers: History, Status, Potential. *Appl. Sci.* **2021**, *11*, 7539. [CrossRef]
37. Xiao, Y.; Brunet, F.; Kanskar, M.; Faucher, M.; Wetter, A.; Holehouse, N. 1-kilowatt CW all-fiber laser oscillator pumped with wavelength-beam-combined diode stacks. *Opt. Express* **2012**, *20*, 3296. [CrossRef]
38. Yu, H.L.; Wang, X.L.; Tao, R.M.; Zhou, P.; Chen, J.B. 1.5 kW, near diffraction-limited, high-efficiency, single-end-pumped all-fiber-integrated laser oscillator. *Appl. Opt.* **2014**, *53*, 8055. [CrossRef] [PubMed]
39. Mashiko, Y.; Nguyen, H.K.; Kashiwagi, M.; Kitabayashi, T.; Shima, K.; Tanaka, D. 2 kW single-mode fiber laser with 20-m long delivery fiber and high SRS suppression. *Proc. SPIE* **2015**, *9728*, 29–34.
40. Shi, W.; Fang, Q.; Xu, Y.; Qin, Y.G.; Fan, J.L.; Meng, X.J.; Zhang, Q.H. 1.63 kW monolithic continuous-wave single-mode fiber laser oscillator. *J Optoelectron. Laser* **2015**, *26*, 662.
41. Yang, B.L.; Zhang, H.W.; Shi, C.; Wang, X.L.; Zhou, P.; Xu, X.J.; Chen, J.B.; Liu, Z.J.; Lu, Q.S. Mitigating transverse mode instability in all fiber laser oscillator and scaling power up to 2.5 kW employing bidirectional-pump scheme. *Opt. Express* **2016**, *24*, 27828. [CrossRef] [PubMed]

42. Ikoma, S.; Nguyen, H.K.; Kashiwagi, M.; Uchiyama, K.; Shima, K.; Tanaka, D. 3 kW single stage all-fiber Yb-doped single-mode fiber laser for highly reflective and highly thermal conductive materials processing. *Proc. SPIE* **2017**, *10083*, 45–50.
43. Kensuke, S.; Shinya, I.; Keisuke, U.; Yuya, T.; Masahiro, K.; Daiichiro, T. 5-kW single stage all-fber Yb-doped single-mode fiber laser for materials processing. *Proc. SPIE* **2018**, *10512*, 45–50.
44. Yang, B.L.; Zhang, H.W.; Shi, C.; Tao, R.M.; Su, R.T.; Ma, P.F.; Wang, X.L.; Zhou, P.; Xu, X.J.; Lu, Q.S. 3.05 kW monolithic fiber laser oscillator with simultaneous optimizations of stimulated Raman scattering and transverse mode instability. *J. Opt.* **2018**, *20*, 025802. [CrossRef]
45. Yang, B.L.; Zhang, H.W.; Ye, Q.; Pi, H.Y.; Shi, C.; Tao, R.M.; Wang, X.L.; Xu, X.J. 4.05 kW monolithic fiber laser oscillator based on home-made large mode area fiber Bragg gratings. *Chin. Opt. Lett.* **2018**, *16*, 031407. [CrossRef]
46. Krämer, R.G.; Möller, F.; Matzdorf, C.; Goebel, T.A.; Strecker, M.; Heck, M.; Richter, D.; Plötner, M.; Schreiber, T.; Tünnermann, A.; et al. Extremely robust femtosecond written fiber Bragg gratings for an ytterbium-doped fiber oscillator with 5 kW output power. *Opt. Lett.* **2020**, *45*, 1447. [CrossRef]
47. Wang, Y.; Kitahara, R.; Kiyoyama, W.; Shirakura, Y.; Kurihara, T.; Nakanish, Y.; Yamamoto, T.; Nakayama, M.; Ikoma, S.; Shima, K. 8-kW single-stage all-fiber Yb-doped fiber laser with a BPP of 0.50 mm-mrad. *Proc. SPIE* **2020**, *11260*, 273–278.
48. Xi, X.M.; Wang, P.; Yang, B.L.; Wang, X.L.; Zhang, H.W.; Ning, Y.; Han, K.; Wang, Z.F.; Zhou, P.; Xu, X.J.; et al. The output power of the all-fiber laser oscillator exceeds 7 kW. *Chin. J. Lasers* **2021**, *48*, 0116001.
49. Nikolai, P.; Oleg, S.; Valentin, F.; Daniil, M.; Roman, Y.; Anton, F.; Alexey, D.; Ivan, U.; Valentin, G. High-efficient kW-level single-mode ytterbium fiber lasers in all-fiber format with diffraction-limited beam at wavelengths in 1000–1030 nm spectral range. *Proc. SPIE* **2020**, *11260*, 1126003.
50. Kotov, L.V.; Likhachev, M.E.; Bubnov, M.M.; Medvedkov, O.I.; Yashkov, M.V.; Guryanov, A.N.; Lhermite, J.; Février, S.; Cormier, E. 75 W 40% efficiency single-mode all-fiber erbium-doped laser cladding pumped at 976 nm. *Opt. Lett.* **2013**, *38*, 2230. [CrossRef] [PubMed]
51. Jebali, M.A.; Maran, J.N.; Larochelle, S. 264 W output power at 1585 nm in Er-Yb co-doped fiber laser using in-band pumping. *Opt. Lett.* **2014**, *39*, 3974. [CrossRef] [PubMed]
52. Kotov, L.V.; Likhachev, M.E.; Bubnov, M.M.; Medvedkov, O.I.; Yashkov, M.V.; Guryanov, A.N.; Février, S.; Lhermite, J.; Cormier, E. Yb-free Er-doped all-fiber amplifier cladding-pumped at 976 nm with output power in excess of 100 W. *Proc. SPIE* **2014**, *8961*, 149–154.
53. Daniel, C.; Herman, P.; Julia, L.; Scott, D.S. Single frequency 1560 nm Er:Yb fiber amplifier with 207 W output power and 50.5% slope efficiency. *Proc. SPIE* **2016**, *9728*, 426–431.
54. De Varona, O.; Fittkau, W.; Booker, P.; Theeg, T.; Steinke, M.; Kracht, D.; Neumann, J.; Wessels, P. Single-frequency fiber amplifier at 1.5 µm with 100 W in the linearly-polarized TEM00 mode for next-generation gravitational wave detectors. *Opt. Express.* **2017**, *25*, 24880. [CrossRef] [PubMed]
55. Han, Q.; Yao, Y.Z.; Tang, X.Y.; Chen, Y.F.; Yan, W.C.; Liu, T.G.; Song, H.L. Highly efficient Er–Yb co-doped double-clad fiber amplifier with an Yb-band resonant cavity. *Laser Phys. Lett.* **2017**, *14*, 025105. [CrossRef]
56. Lin, H.Q.; Feng, Y.J.; Feng, Y.T.; Barua, P.; Sahu, J.K.; Nilsson, J. 656 W Er-doped, Yb-free large-core fiber laser. *Opt. Lett.* **2018**, *43*, 3080. [CrossRef]
57. Matniyaz, T.; Kong, F.; Kalichevsky-Dong, M.T.; Dong, L. 302 W single-mode power from an Er/Yb fber MOPA. *Opt. Lett.* **2020**, *45*, 2910. [CrossRef]
58. Michaud, L.-C.; Veilleux, C.; Bilodeau, G.; Paquet, O.; Lebel-Cormier, M.-A.; Lemieux-Tanguay, M.; Pelletier-Ouellet, S.; Paradis, P.; Bellec, M.; Grégoire, N.; et al. 100-W-level single-mode ytterbium-free erbium fiber laser. *Opt. Lett.* **2021**, *46*, 2553. [CrossRef]
59. Yu, W.L.; Xiao, Q.R.; Wang, L.L.; Zhao, Y.; Qi, T.C.; Yan, P.; Gong, M.L. 219.6 W large-mode-area Er: Yb co-doped fiber amplifier operating at 1600 nm pumped by 1018 nm fiber lasers. *Opt. Lett.* **2021**, *46*, 2192. [CrossRef]
60. Yu, W.L.; Yan, P.; Qi, T.C.; Wu, Y.L.; Li, D.; Xiao, Q.R.; Gong, M.L. Highpower and high-brightness Er: Yb co-doped fiber MOPA operating at 1535 nm. *Opt. Express* **2022**, *30*, 16837. [CrossRef]
61. Li, W.; Qiu, Q.; Yu, L.; Gu, Z.; He, L.; Liu, S.; Yin, X.; Zhao, X.; Peng, J.; Li, H.; et al. Er/Yb co-doped 345-W all-fiber laser at 1535 nm using hybrid fiber. *Opt. Express* **2023**, *48*, 3027–3030. [CrossRef]
62. Stutzki, F.; Gaida, C.; Gebhardt, M.; Jansen, F.; Wienke, A.; Zeitner, U.; Fuchs, F.; Jauregui, C.; Wandt, D.; Kracht, D.; et al. 152 W average power Tm-doped fiber CPA system. *Opt. Lett.* **2014**, *39*, 4671. [CrossRef] [PubMed]
63. Walbaum, T.; Heinzig, M.; Schreiber, T.; Eberhardt, R.; Tünnermann, A. Monolithic thulium fiber laser with 567 W output power at 1970 nm. *Opt. Lett.* **2016**, *41*, 2632. [CrossRef] [PubMed]
64. Yin, K.; Zhu, R.Z.; Zhang, B.; Liu, G.C.; Zhou, P.; Hou, J. 300 W-level, wavelength-widely-tunable, all-fber integrated thulium-doped fiber laser. *Opt. Express* **2016**, *24*, 11085. [CrossRef]
65. Jiang, L.; Chen, L.; Xing, S.H.; Pu, W. 342 W narrow-linewidth continuous-wave thulium-doped all-fber laser. *Acta. Phys. Sin.* **2016**, *65*, 194209. [CrossRef]
66. Gaida, C.; Gebhardt, M.; Heuermann, T.; Stutzki, F.; Jauregui, C.; Limpert, J. Ultrafast thulium fber laser system emitting more than 1 kW of average power. *Opt. Lett.* **2018**, *43*, 5853. [CrossRef] [PubMed]
67. Yao, W.C.; Shen, C.F.; Shao, Z.H.; Wang, J.L.; Wang, F.; Zhao, Y.G.; Shen, D.Y. 790 W incoherent beam combination of a Tm-doped fiber laser at 1941 nm using a 3 × 1 signal combiner. *Appl. Opt.* **2018**, *57*, 5574. [CrossRef] [PubMed]

68. Liu, Y.Z.; Cao, C.; Xing, Y.B.; Liao, L.; Cao, R.T.; Zhang, F.F.; Chen, Y.S.; Wang, Y.B.; Peng, J.G.; Li, H.Q.; et al. 406 W narrow-linewidth all-fiber amplifier with Tm-doped fiber fabricated by MCVD. *IEEE Photonics Technol. Lett.* **2019**, *31*, 1779. [CrossRef]
69. Zi, L.Y.; Bing, X.Y.; Lei, L.; Bo, W.Y.; Gang, P.J.; Qing, L.H.; Li, D.N.; Yan, L.J. 530 W all-fiber continuous-wave Tm-doped fiber laser. *Acta. Phys. Sin.* **2020**, *69*, 184209.
70. Motard, A.; Louot, C.; Robin, T.; Cadier, B.; Manek-Hönninger, I.; Dalloz, N.; Hildenbrand-Dhollande, A. Diffraction limited 195-W continuous wave laser emission at 2.09 µm from a Tm^{3+}, Ho^{3+} co-doped single-oscillator monolithic fiber laser. *Opt. Express* **2021**, *29*, 6599. [CrossRef]
71. Ren, C.; Shen, Y.; Zheng, Y.; Mao, Y.; Wang, F.; Shen, D.; Zhu, H. Widely-tunable all-fiber Tm doped MOPA with > 1 kW of output power. *Opt. Express* **2023**, *2931*, 22733–22739. [CrossRef] [PubMed]
72. Alexander, H.; Nikita, S.; John, H.; Adrian, C. High power resonantly pumped holmium-doped fiber sources. *Proc. SPIE* **2014**, *8982*, 898292.
73. IPG Photonics. "High Power CW Fiber Lasers". (IPG Photonics). Available online: https://www.ipgphotonics.com/en/products/lasers/highpower-cw-fiber-lasers (accessed on 8 February 2024).
74. Garmire, E.; Pandarese, F.; Townes, C.H. Coherently driven molecular vibrations and light modulation. *Phys. Rev. Lett.* **1963**, *11*, 160–163. [CrossRef]
75. Vermeulen, N.; Debaes, C.; Muys, P.; Theinpont, H. Mitigating heat dissipation in Raman lasers using coherent anti-Stokes Raman scattering. *Phys. Rev. Lett.* **2007**, *99*, 093903. [CrossRef]
76. Vermeulen, N.; Debaes, C.; Thienpont, H. Mitigating heat dissipation in near- and mid-infrared silicon-based Raman lasers using CARS: I. Theoretical analysis. *IEEE J. Sel. Top. Quantum Electron.* **2007**, *13*, 770–782. [CrossRef]
77. Vermeulen, N.; Debaes, C.; Thienpont, H. Mitigating heat dissipation in near- and mid-infrared silicon-based Raman lasers using CARS: II. Numerical demonstration. *IEEE J. Sel. Top. Quantum Electron.* **2007**, *13*, 783–788. [CrossRef]
78. Bobbs, B.; Warner, C. Raman-resonant four-wave mixing and energy transfer. *J. Opt. Soc. Am. B* **1990**, *7*, 234–238. [CrossRef]
79. Nemova, G.; Caloz, C. Heat Evacuation from Active Raman Media Using Frequency-Selective Dissipative Coupling. *Phys. Rev. Res.* **2021**, *3*, 013050. [CrossRef]
80. Belanger, E.; Bernier, M.; Faucher, D.; Cote, D.; Vallee, R. Highpower and widely tunable all-fiber Raman laser. *J. Light. Technol.* **2008**, *26*, 1696–1701. [CrossRef]
81. Zhang, Y.; Xu, J.; Ye, J.; Song, J.; Yao, T.; Zhou, P. Ultralow-quantum-defect Raman laser based on the boson peak in phosphosilicate fiber. *Photonics Res.* **2020**, *8*, 1155–1160. [CrossRef]
82. Dong, J.; Zhang, L.; Zhou, J.; Pan, W.; Gu, X.; Feng, Y. More than 200 W random Raman fiber laser with ultra-short cavity length based on phosphosilicate fiber. *Opt. Lett.* **2019**, *44*, 1801–1804. [CrossRef] [PubMed]
83. Tanaka, H.; Shintani, H. Universal link between the boson peak and transverse phonons in glass. *Nat. Mater.* **2008**, *7*, 870–877.
84. Glick, Y.; Shamir, Y.; Wolf, A.A.; Dostovalov, A.V.; Babin, S.A.; Pearl, S. Highly efficient all-fiber continuous-wave Raman graded-index fiber laser pumped by a fiber laser. *Opt. Lett.* **2018**, *43*, 1027–1030. [CrossRef]
85. Glick, Y.; Shamir, Y.; Aviel, M.; Sintov, Y.; Goldring, S.; Shafir, N.; Pearl, S. 1.2 kW clad pumped Raman all-passive-fiber laser with brightness enhancement. *Opt. Lett.* **2018**, *43*, 4755–4758. [CrossRef]
86. Chen, Y.; Leng, J.; Xiao, H.; Yao, T.; Zhou, P. Pure passive fiber enabled highly efficient Raman fiber amplifier with record kilowatt power. *IEEE Access* **2019**, *7*, 28334–28339. [CrossRef]
87. Brillouin, L. Diffusion de la lumière et des Rayons X par un corps transparent homogène. *Ann. Phys.* **1922**, *9*, 88–122. [CrossRef]
88. Mandelstam, L. Light scattering by inhomogeneous media. *Zh. Russ. Fiz-Khim.* **1926**, *58*, 381.
89. Chiao, R.; Townes, C.; Stoicheff, B. Stimulated Brillouin scattering and coherent generation of intense hypersonic waves. *Phys. Rev. Lett.* **1964**, *12*, 592–595. [CrossRef]
90. Hill, K.O.; Kawasaki, B.S.; Johnson, D.C. CW Brillouin laser. *Appl. Phys. Lett.* **1976**, *28*, 608–609. [CrossRef]
91. Shee, Y.G.; Al-Mansoori, M.H.; Yaakob, S.; Man, A.; Zamzuri, A.K.; Mahamd Adikan, F.R.; Mahdi, M.A. Millimeter wave carrier generation based on a double-Brillouin-frequency spaced fiber laser. *Opt. Express* **2012**, *20*, 13402–13408. [CrossRef]
92. Abass, A.K.; Al-Mansoori, M.H.; Jamaludin, M.Z.; Abdullah, F.; Al-Mashhadani, T.F.; Ali, M.H. L-band multi-wavelength brillouin-raman fber laser with 20-GHz channel spacing. *Fiber Integr. Opt.* **2014**, *33*, 56–67. [CrossRef]
93. Al-Mashhadani, T.F.; Al-Mashhadani, M.K.S.; Yucel, M.; Goktas, H.H. Influence of bidirectional cavity structure on the Brillouin Stokes signal characteristics in ring BFL. *Optik* **2019**, *185*, 359–363. [CrossRef]
94. Al-Mansoori, M.H.; Al-Sheriyani, A.; Al-Nassri, S.; Hasoon, F.N. Generation of efficient 33 GHz optical combs using cascaded stimulated Brillouin scattering effects in optical fiber. *Laser Phys.* **2017**, *27*, 65112. [CrossRef]
95. Al-Mansoori, M.H.; Al-Sheriyani, A.; Younis, M.A.A.; Mahdi, M.A. Widely tunable multiwavelength Brillouin-erbium fiber laser with triple Brillouin-shift wavelength spacing. *Opt. Fiber Technol.* **2018**, *41*, 21–26. [CrossRef]
96. Al-Mashhadani, T.F. Erbium gain effects on Stokes signal performance in a Fabry-Perot Brillouin Erbium fiber laser. *Opt. Quantum Electron.* **2019**, *51*, 189. [CrossRef]
97. Al-Mashhadani, T.F.; Al-Mashhadani, M.K.S.; Goktas, H.H.; Yucel, M.; Celebi, F.V. Widely triple Brillouin frequency shift multiwavelength Brillouin erbium fiber laser. *Opt. Quantum* **2020**, *52*, 288. [CrossRef]
98. Al-Mashhadani, M.K.S.; Al-Mashhadani, T.F.; Goktas, H.H. Tunable 50 GHz laser comb generation of multiwavelength Brillouin erbium fber laser. *Opt. Commun.* **2020**, *464*, 125542. [CrossRef]

99. Awsaj, M.K.; Al-Mashhadani, T.F.; Al-Mashhadani, M.K.S.; Ali, A.Y.; Zan, M.S.D.; Arsad, N. Multiwavelength fiber laser sources with 60 GHz Brillouin frequency shift. *Opt. Quantum Electron.* **2023**, *55*, 528. [CrossRef]
100. Shi, Y.; Wang, T.; Hao, Y.-Z.; Bai, H.-Y.; Yang, Y.-D.; Xiao, J.-L.; Chen, Y.-L.; Huang, Y.-Z. Wideband multiwavelength Brillouin fiber laser with switchable channel spacing. *Appl. Opt.* **2023**, *62*, 2130–2136. [CrossRef]
101. Silva, L.C.B.; Segatto, M.E.V. Advances in multi-wavelength Brillouin fiber lasers: An outlook across different spectral regions. *Opt. Fiber Technol.* **2023**, *76*, 103246. [CrossRef]
102. Bashan, G.; Diamandi, H.H.; Zehavi, E.; Sharma, K.; London, Y.; Zadok, A. A forward Brillouin fibre laser. *Nat Commun.* **2022**, *13*, 3554. [CrossRef]
103. Sobih, M.; Crouse, P.L.; Li, L. Elimination of striation in laser cutting of mild steel. *J. Phys. D Appl. Phys.* **2007**, *40*, 6908–6916. [CrossRef]
104. Wagner, F.; Grupp, M.; Vollertsen, F. Laser beam micro welding with single mode fibre lasers. In Proceedings of the Third International WLT-Conference on Lasers in Manufacturing (LIM), Munich, Germany, 13–16 June 2005; pp. 769–772.
105. Ludewigt, K.; Liem, A.; Stuhr, U.; Jung, M. High-power laser development for laser weapons. In *Hogh Power Lasers: Technology and Systems, Platforms, Effects III*; SPIE: Strasbourg, France, 2019; Volume 11162, pp. 46–53.
106. Baac, H.W.; Uribe-Patarroyo, N.; Bouma, B.E. High-energy pulsed Raman fiber laser for biological tissue coagulation. *Opt. Express* **2014**, *22*, 7113–7123. [CrossRef] [PubMed]
107. Yan, P.; Xu, W.; Hu, H.; Zhang, Z.; Li, Z.; Shu, R. Recent advances, applications, and perspectives in erbium-doped fiber combs. *Photonics* **2024**, *11*, 192. [CrossRef]
108. Sheremet, A.S.; Petrov, M.I.; Iorsh, I.V.; Poshakinskiy, A.P.; Poddubny, A.N. Waveguide quantum electrodynamics: Collective radiance and photon-photon correlations. *Rev. Mod. Phys.* **2023**, *95*, 015002. [CrossRef]
109. Dragic, P.D.; Cavillon, M.; Ballato, J. Materials for optical fiber lasers: A review. *Appl. Phys. Rev.* **2018**, *5*, 041301. [CrossRef]